# Systematic study of particle production in $p+p$ ($\bar{p}$) collisions via the HIJING model

Xin-Nian Wang* and Miklos Gyulassy
*Nuclear Science Division, Mailstop 70A-3307, Lawrence Berkeley Laboratory, University of California, Berkeley, California 94720*
(Received 16 September 1991)

We apply the newly developed HIJING Monte Carlo model to perform a systematic study of a broad range of data on $p+p(\bar{p})$ collisions. The model combines a simple string phenomenology for low-$p_T$ processes together with perturbative QCD for high-$p_T$ processes. We emphasize the effects due to multiple-minijet production at collider energies. The energy and multiplicity dependence of charged particle rapidity and transverse momentum spectra, the Koba-Nielsen-Olesen violation of multiplicity distributions, and the two-particle correlation functions are shown to be simultaneously well accounted for with this model.

PACS number(s): 13.87.Ce, 12.40.Aa, 13.85.Hd

## I. INTRODUCTION

Multiple minijets with $p_T \sim$ few GeV in ultrarelativistic heavy-ion collisions have been estimated [1] to play an important role at BNL Relativistic Heavy Ion Collider (RHIC) ($\sqrt{s} \sim 200$ GeV/nucleon) and CERN Large Hadron Collider (LHC) ($\sqrt{s} \sim 6$ TeV/nucleon) energies. While not resolvable as distinct jets, they are expected to lead to a wide variety of correlations among observables that compete with some of the suggested signatures of a quark-gluon plasma (QGP) [2], which may be formed during such collisions. To study the background due to minijets and to test proposed signatures and probes of ultradense matter such as jet quenching [3], we have developed a Monte Carlo model HIJING (heavy ion jet interaction generator) [4]. The model includes multiple minijet production, nuclear shadowing of parton distribution functions, and jet interaction in an excited nuclear matter.

Though multiple minijets and the associated nuclear effects such as parton shadowing and jet quenching have only been recently addressed [4], the need to include jet production in hadron induced interactions and particle production is well known. It had been suggested by many authors that jet production could be responsible for various phenomena in high energy hadronic interactions such as the increase of the total $pp$ and $p\bar{p}$ cross sections with energy [5–11], the correlation between averaged transverse momentum and charged multiplicity [6,8,12], and the violation of Koba-Nielsen-Olesen (KNO) scaling of charged multiplicity distributions [8,13,14]. Several Monte Carlo models [15–19] have also been developed to take into account semihard processes in $pp$ and $p\bar{p}$ collisions. However, to the best of our knowledge, PYTHIA [18] is the only one that incorporates the perturbative QCD (PQCD) approach to multiple-jet processes including initial and final state radiation in minimum-biased events of hadronic interactions. The dual parton model (DPM) [15], with cut Pomerons playing a similar role equivalent to multiple minijets, is based on nonperturbative phenomenology. ISAJET [17] is designed only for the study of large-$p_T$ jets with an independent beam-jet fragmentation scheme. Gaisser and Stanev considered multiple minijet production in Ref. [19] in a more simplified scheme. FRITIOF [16] utilizes the PYTHIA model to simulate hard jet production in addition to a phenomenological ansatz for soft gluon bremsstrahlung.

The formulation of HIJING [4] was guided by the successful implementation of PQCD in PYTHIA [18] and the need to develop a consistent model of soft processes. We calculate all cross sections in the framework of the eikonal formalism as outlined in Refs. [9,14,19]. In addition, HIJING also incorporates a version of the multistring phenomenology of DPM and FRITIOF models for low-$p_T$ interactions, thus providing a link between the dominant nonperturbative fragmentation physics at intermediate energies and the perturbative physics at collider energies. In order to extend the model to $pA$ and $AA$ reactions as well, some of the nuclear effects of initial and final state interactions have also been taken into account. In Refs. [4,20], we studied in detail the nuclear dependence of multiparticle production in heavy ion collisions.

In this paper, we apply HIJING to study systematically particle production in $pp$ and $p\bar{p}$ collisions and to check the consistency of the model with experimental data over a wide energy range. It is necessary to look at the whole spectrum of data on $pp$ and $p\bar{p}$ collisions at one time in order to develop a better understanding of the underlying dynamics of particle production. Not only the global features of the reaction but also the detailed inclusive distributions, correlations, and fluctuations of particle production need to be understood in terms of one consistent model. Given the suggested importance of multiple minijets [5–14] in hadronic interactions at collider energies, one goal of this paper is to study the intricate correlations among observables due to the interplay between the nonperturbative low-$p_T$ physics and the perturbative multiple minijet physics. We show how multiple minijets emerge and become a prominent and integral part of ha-

*Present address: Department of Physics, Duke University, Durham, NC 27706.

 ©1992 The American Physical Society

dronic interactions. In addition, this study is needed to develop increased confidence in the extrapolation of the model to $pA$ and $AA$ collisions where it is essential to disentangle nuclear effects such as nuclear shadowing of gluon distribution function and jet quenching [20].

The outline of this paper is as follows. Section II gives a brief review of the HIJING model as discussed in detail in Ref. [4]. Emphasis will be on the aspects of the model specific to hadronic interactions. In Secs. III and IV, we study the inclusive single particle distributions in rapidity and transverse momentum. Both the energy and multiplicity dependence of the multiparticle production are discussed. Charged multiplicity distributions of non-single-diffractive events are discussed in Sec. V. The underlying event structure of multiple minijet production and the violation of KNO scaling are illustrated. In Sec. VI, we consider the flavor composition of particle production. Both short and long range two particle correlations in different rapidity bins and their implications are discussed in Sec. VII. Finally, Sec. VIII concludes with a summary and some general remarks.

Throughout this paper, we refer to the number of jets as the number of parton-parton scatterings with $p_T$ transfer larger than a minimum scale $p_0$ which we specify below.

## II. THE HIJING MODEL

Since the HIJING model has been discussed in detail in Ref. [4], we give here only a brief review of the aspects relevant to hadronic interactions. HIJING includes the following features.

(1) Multiple minijet production with initial and final state radiation is included along the lines of the PYTHIA model [18] with cross sections calculated with the eikonal formalism. For triggered high-$p_T$ processes, the associated enhancement of semihard and soft background is calculated self-consistently.

(2) Soft beam jets are modeled by quark-diquark strings with gluon kinks along the lines of the FRITIOF model and the DPM model [15,16]. In addition, multiple low-$p_T$ exchanges among the end point constituents are included.

(3) Exact diffuse nuclear geometry is used to calculate the impact parameter dependence of the number of inelastic processes [21].

(4) An impact parameter dependent parton structure function is introduced to study the sensitivity of observables to nuclear shadowing, especially of the gluon structure functions.

(5) A model for jet quenching is included to enable the study of the $A$ dependence of moderate- and high-$p_T$ observables on an assumed energy loss of partons traversing the produced dense matter.

The rate of multiple minijet production in HIJING is constrained by the cross sections in nucleon-nucleon collisions. Within an eikonal formalism [5–11], the cross sections can be expressed as

$$\sigma_{\rm el}=\pi\int_0^\infty db^2[1-e^{-\chi(b,s)}]^2 , \tag{1}$$

$$\sigma_{\rm in}=\pi\int_0^\infty db^2[1-e^{-2\chi(b,s)}] , \tag{2}$$

$$\sigma_{\rm tot}=2\pi\int_0^\infty db^2[1-e^{-\chi(b,s)}] , \tag{3}$$

in the limit that the real part of the scattering amplitude can be neglected and thus that the eikonal function $\chi(b,s)$ at an impact parameter $b$ is real. As in Ref. [14], the eikonal function is modeled as

$$\chi(b,s)\equiv\chi_s(b,s)+\chi_h(b,s) =\chi_0(\xi)+\chi_0(\xi)\frac{\sigma_{\rm jet}(s)}{\sigma_{\rm soft}(s)} , \tag{4}$$

with

$$\chi_0(\xi)=\frac{\mu_0^2}{48}(\mu_0\xi)^3K_3(\mu_0\xi),\quad \xi=b/b_0(s) , \tag{5}$$

where $\mu_0=3.9$ and $\pi b_0^2(s)\equiv\sigma_{\rm soft}(s)/2$ providing a measure of the geometrical size of the nucleon. This form of eikonal function ensures that geometrical scaling [22] is recovered when $\sigma_{\rm jet}\ll\sigma_{\rm soft}$ at low energies. Here $\sigma_{\rm soft}$, which we regard as a parameter, is the nonperturbative inclusive cross section for soft processes. $\sigma_{\rm jet}$ is the total inclusive cross section for hard or semihard parton scatterings above a $p_T$ cutoff $p_0$ in the PQCD parton model:

$$\sigma_{\rm jet}=\int_{p_0^2}^{s/4}dp_T^2\,dy_1\,dy_2\frac{1}{2}\frac{d\sigma_{\rm jet}}{dp_T^2\,dy_1\,dy_2} , \tag{6}$$

where $y_1,y_2$ are the rapidities of the two final partons. The differential dijet cross section $d\sigma_{\rm jet}$ can be written as [23]

$$\frac{d\sigma_{\rm jet}}{dp_T^2\,dy_1\,dy_2}=K\sum_{a,b}x_1f_a(x_1,p_T^2)x_2f_b(x_2,p_T^2) \times d\sigma^{ab}(\hat{s},\hat{t},\hat{u})/d\hat{t} , \tag{7}$$

with the summation running over all partons species, where $x_1$ and $x_2$ are the light-cone momentum fractions carried by the initial partons. The variables are related by $x_1=x_T(e^{y_1}+e^{y_2})/2$, $x_2=x_T(e^{-y_1}+e^{-y_2})/2$, $x_T=2p_T/\sqrt{s}$. The PQCD cross sections $d\sigma_{ab}$ depend on the subprocess variables $\hat{s}=x_1x_2s$, $\hat{t}=-p_T^2[1+\exp(y_2-y_1)]$, and $\hat{u}=-p_T^2[1+\exp(y_1-y_2)]$. In HIJING, the structure functions $f_a(x,Q^2)$ are taken to be Duke-Owens [24] parametrized structure function set 1. This parametrization for $f_a(x,Q^2)$, is adequate through the CERN Collider energies. For higher energies the Eichten-Hinchliffe-Lane-Quigg (EHLQ) [23] or Harriman-Martin-Stirling-Roberts (HMSR) [25] parametrization can be used. A factor $K\approx2$ is included to correct the lowest order PQCD rates for next-to-leading order effects.

Though the cross sections for more than two parton production can be estimated perturbatively [26], we take a probabilistic approach [9,14,13] to multiple independent minijet production. In our framework, the cross sections for no and $j\geq1$ number of jet production with $p_T>p_0$ are

$$\sigma_0=\pi\int_0^\infty db^2[1-e^{-2\chi_s(b,s)}]e^{-2\chi_h(b,s)}, \tag{8}$$

$$\sigma_j=\pi\int_0^\infty db^2\frac{[2\chi_h(b,s)]^j}{j!}e^{-2\chi_h(b,s)}. \tag{9}$$

Their sum gives rise to the total inelastic cross section $\sigma_{\rm in}$ as in Eq. (2).

Choosing $p_0\simeq 2$ GeV/$c$ and assuming a constant value of $\sigma_{\rm soft}=57$ mb at high energies, the calculated total, elastic, and inelastic cross sections in $pp$ or $p\bar{p}$ collisions agree well with experiments [27–32] from CERN Intersecting Storage Ring (ISR) to cosmic-ray energies as shown in Fig. 1. We note that the total inclusive jet cross section, shown as a dashed line in the figure, increases much faster than the total cross section as a function of $\sqrt{s}$, implying that the average number of minijets, $\sigma_{\rm jet}/\sigma_{\rm in}$, also increases at high energies. As we will show later in this paper, this energy dependence is a major cause of many phenomena in particle production at collider energies. The geometrical scaling, e.g., a constant $\sigma_{\rm el}/\sigma_{\rm tot}$ ratio, which we have achieved at low energies, is also broken by the onset of $\sigma_{\rm jet}$ with increasing energy [14].

In HIJING, once the cross sections and the number of minijets are determined as described above, PYTHIA subroutines [18] are used to generate the kinetic variables of the scattered partons, including the initial and final state radiation associated with each hard scattering. The remaining energy of the colliding system after the minijet production is then used for the soft process. The soft process has a collective longitudinal-momentum exchange between the valence quarks, leading to two excited strings stretching between quarks and diquarks. The soft processes also involve an extra low $p_T<p_0$ transverse-momentum transfer to the constituent quarks and diquarks at the string end points. Following FRITIOF, HIJING also includes soft gluon bremsstrahlung to soft processes. However, unlike FRITIOF which extends the soft radiation to high $p_T$, HIJING restricts the radiation to $p_T<p_0$. This limitation is natural for induced gluon bremsstrahlung due to soft exchanges [33]. The produced gluons from minijet production are represented as kinks, as in the Lund model [34], on the two excited strings with their specified large or intermediate $p_T$ along with those low-$p_T$ gluons from the induced soft radiations. If a valence quark is involved in a hard scattering, the string end point of this quark will carry the transverse-momentum transfer of that hard process. Finally, the excited strings with their associated gluon kinks are fragmented into hadrons according to Lund JETSET7.2 [34] fragmentation scheme.

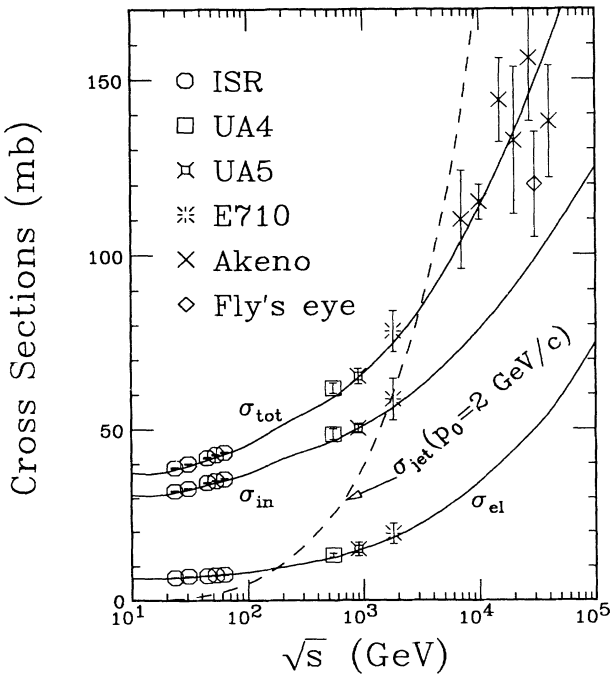


FIG. 1. The total, inelastic, and elastic cross sections of $pp$ and $p\bar{p}$ collisions as calculated by HIJING (solid lines). The data are from Refs. [27–32]. The dashed line is the total inclusive jet cross section with $p_T\geq p_0=2$ GeV/$c$.

## III. RAPIDITY DISTRIBUTIONS

In the following sections we study particle production in $pp$ and $p\bar{p}$ collisions in a wide energy range, from $\sqrt{s}\approx 5$ GeV up to Fermilab Tevatron energy $\sqrt{s}=1800$ GeV and discuss in detail the parameters of the model needed to achieve the overall agreement with the experimental data. All the calculation results we show here are obtained with one consistent set of (default) parameters. Much of the data we consider here have already been studied separately by different authors [15,16,18,19]. However, our intention in this paper is to consider all the data simultaneously in terms of one consistent model. Our goal is to form a global picture of multiparticle production and to test the role of multiple minijet production in much greater detail than possible before.

The rapidity and pseudorapidity of a particle are defined as

$$y=\frac{1}{2}\ln\frac{E+p_L}{E-p_L}, \tag{10}$$

$$\eta=\frac{1}{2}\ln\frac{p+p_L}{p-p_L}, \tag{11}$$

respectively, with $p_L$ as the momentum component in the beam direction. Shown in Fig. 2 are the calculated inclusive rapidity distributions, $\rho(y)=(1/\sigma)d\sigma/dy$, of produced particles in $pp$ collisions at $E_{\rm lab}=24$ and 200 GeV. The corresponding data are from Refs. [35,36]. From Fig. 1 we can see that jet production is negligible at energies $\sqrt{s}<20$ GeV. The dominant processes are soft interactions which are modeled by two string excitations in HIJING. Since the longitudinal momenta of the valence quarks and diquarks at string end points are proportional to the incident momentum, the rapidity lengths of the excited strings increase with beam energy leading to a wider rapidity distribution of produced particles. The increase of central rapidity density in Fig. 2 is mainly due to the overlapping of two strings with finite rapidity lengths at low energies. As we will see later, the central rapidity

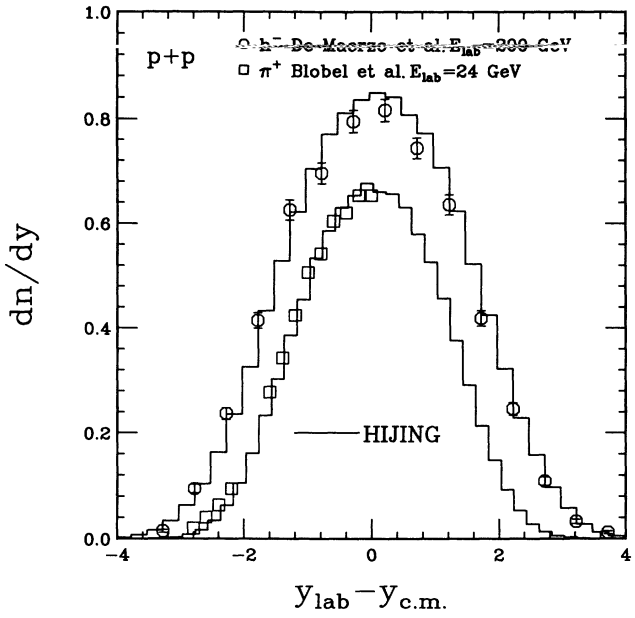


FIG. 2. Rapidity distributions of $\pi^+$ in $pp$ collisions at $E_{\rm lab}=24$ GeV and negative particles at $E_{\rm lab}=200$ GeV. The histograms are HIJING results and data points are from Refs. [35,36].

density of produced particles from the two excited strings in soft processes saturates and remains constant as the colliding energy increases.

In HIJING, we have assumed a probability

$$P(x)\sim 1/x \ , \tag{12}$$

for fractional light-cone momentum exchange in single-diffractive excitations. By single-diffractive excitation we mean that only one of the colliding nucleons becomes an excited string. These events occur with a parametrized cross section as empirically determined in Ref. [37]. The assumption of Eq. (12) is guided by the distribution proposed in FRITIOF [16] and it reproduces well the $dM/M$ distribution observed in single-diffractive events [37]. In FRITIOF, the same distribution is used for non-single-diffractive excitations. This scheme is consistent with data at low energies. However, at higher collider energies we find that it gives too wide a rapidity distribution for produced particles. We therefore have chosen instead a probability distribution

$$P(x)\sim(1-x)^{3/2}/\sqrt{x} \ , \tag{13}$$

in non-single-diffractive excitations as used in the DPM [15]. With the above assumption, the pseudorapidity distributions of charged particles are in good agreement with the energy dependence of the collider data [38,39] as shown in Fig. 3. HIJING (histograms) reproduces both the overall widening of the distribution and the increase of central density with the colliding energy. Note that the dip at $\eta=0$ is purely kinematical. Both the calculation and data shown in Fig. 3 are for non-single-diffractive (NSD) events selected according to the corresponding experimental triggers. Here, the NSD triggers require at least one charged particle simultaneously in each of the pseudorapidity regions at both ends covering $2<|\eta|<5.6$ for UA5 data, and $3.2<|\eta|<5.9$ for Collider Detector at Fermilab (CDF) data. In Fig. 4 we plot HIJING calculation (solid lines) and experimental data [38] on the pseudorapidity distributions of charged particles for inelastic events where only minimum-biased trigger is required. Comparing to the NSD distributions (dashed lines), inelastic events have a reduction of about $\frac{1}{3}$ units in the central density. To obtain the good agreement between data and calculation, the single- and non-single-diffractive string excitations had to be treated differently as noted above.

The increase of central rapidity density with energy is shown in Fig. 5. Both the calculation (solid line) and data [38,40,41] are for inelastic events. The central density for non-single-diffractive events is always above the inelastic ones. The difference decreases within the HIJING model at higher collider energies when the jet cross section is dominant and the probability for single-diffractive string excitations is small. The dashed line in the figure is the calculated central density for those inelastic events without minijet production. Comparing those two curves, we can see that within HIJING a large fraction of produced particles in the central rapidity region come from minijets. The events without minijets, which have only two excited strings from soft interaction, have a constant central rapidity density for the produced particles.

Recalling a previous discussion [14] on the $p_0$ dependence of the soft cross section $\sigma_{\rm soft}$, we note that our

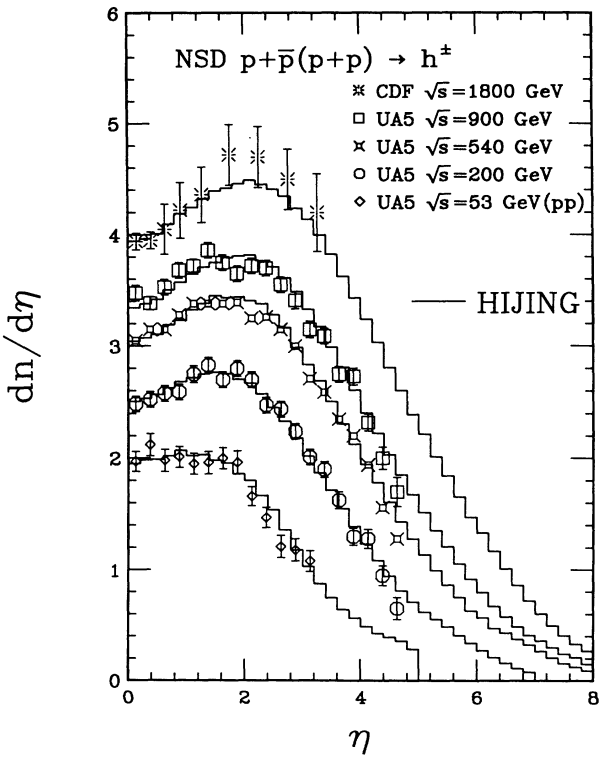


FIG. 3. Pseudorapidity distributions of charged particles in non-single-diffractive $pp$ at $\sqrt{s}=53$ GeV, $p\bar{p}$ collisions at $\sqrt{s}=200$, 540, 900, and 1800 GeV. The data are from Refs. [38,39] and histograms are from HIJING calculations.

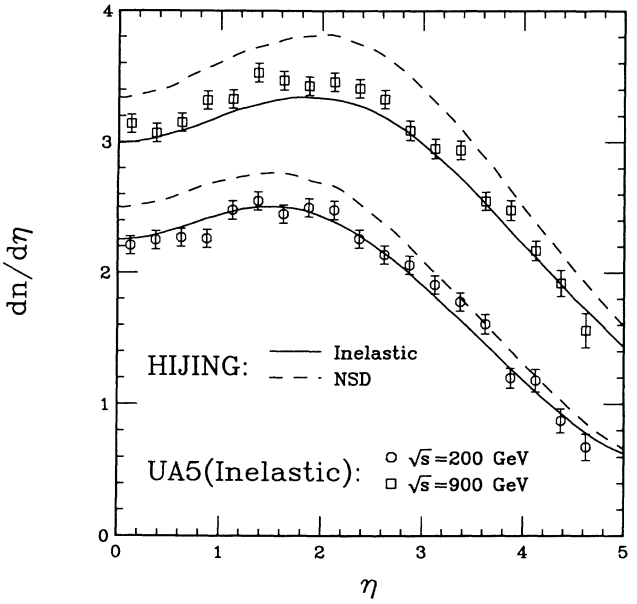


FIG. 4. HIJING calculation (solid lines) and UA5 results [38] of the pseudorapidity distributions of charged particles in inelastic $p\bar{p}$ collisions at $\sqrt{s}=200$ and 900 GeV. The dashed lines are HIJING results for NSD events.

choice of $p_0=2$ GeV is crucial in order to simplify the soft phenomenology. In principle, there is no clear boundary between soft and hard processes. In HIJING, $p_0$ is only a phenomenological scale which divides interactions into nonperturbative soft processes and PQCD hard or semihard processes. There is clearly a correlation between $p_0$ and the required phenomenology of soft processes if we treat hard processes explicitly within PQCD. We find that only with $p_0=2$ GeV can we have a simple framework in which both $\sigma_{\rm soft}$ and the central rapidity density from soft string phenomenology are constant. Otherwise, a more complex scheme for soft processes such as multiple sea-sea strings in the DPM is needed to reproduce the energy dependence of the collider data. Our choice of $p_0=2$ GeV is therefore essential to minimize the uncertainties due to nonperturbative physics and to maximize the domain of applicability of PQCD.

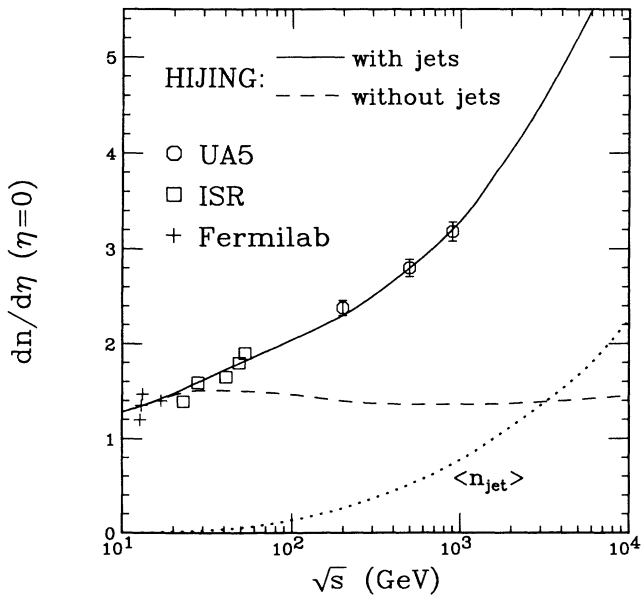


FIG. 5. Central pseudorapidity density at $\eta=0$ of charged particles in inelastic $pp$ and $p\bar{p}$ collisions as a function of $\sqrt{s}$. The solid line is HIJING calculation and the data are from Refs. [38,40,41]. The dashed line is for events without jet production in HIJING simulations. The dotted line is the calculated average number of jet production $\langle n_{\rm jet}\rangle=\sigma_{\rm jet}/\sigma_{\rm in}$.

The correlation between the central density and minijets is very clear when we plot the average number of minijet production (dotted line) $\langle n_{\rm jet}\rangle=\sigma_{\rm jet}/\sigma_{\rm in}$ as a function of $\sqrt{s}$ in the same figure. To elucidate this point, we show in Fig. 6 the semi-inclusive pseudorapidity distributions (solid lines) at two collider energies for events with no jet production, one jet production, and two or more jet production, respectively. We see that the central density is proportional to the number of jet production. For a fixed number of jets, the density is more or less independent of energy, though the width of the distribution increases with $\sqrt{s}$. Therefore, the increase of central rapidity density is totally due to the increase of the number of minijet production at high energies. HIJING thus has a unique prediction about the nonlinear increase of the central density as a function of $\ln(s)$, since the average number of minijets is also a nonlinear function of $\ln(s)$ as shown in Fig. 5.

Associated with jet production, the initial and final state radiation are also taken into account in HIJING through the PYTHIA subroutines. In the study of large $p_T$ jets, they are found to be responsible for the so-called pedestal effect [18,42]. In minimum-biased events, they should also have important effect on particle production. Shown as dashed lines in Fig. 6 are the calculated pseu-

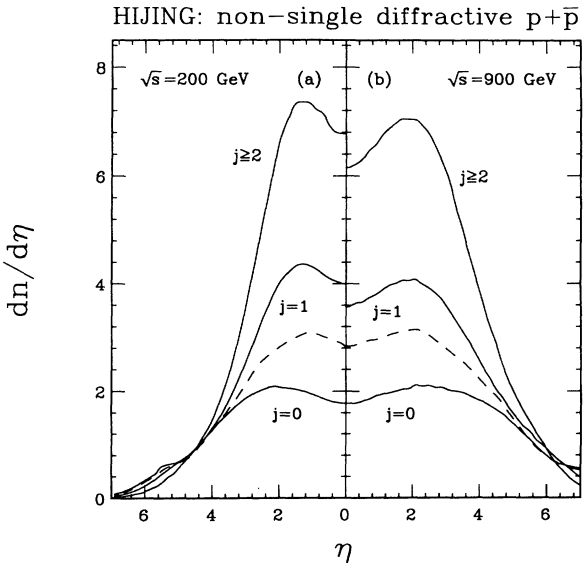


FIG. 6. HIJING calculation of the semi-inclusive pseudorapidity distributions of charged particles in NSD $p\bar{p}$ collisions at (a) $\sqrt{s}=200$ and (b) 900 GeV for events with $j=0$, $j=1$, and $j\geq 2$ number of jet production. The dashed lines are for $j=1$ but without initial and final state radiation.

dorapidity distributions for one jet production events but without initial and final state radiation in HIJING. Comparing to the solid lines with $j=1$, we can see that there is about 25% reduction of the central rapidity density if initial and final state radiation are neglected. This result is consistent with an earlier simple analysis [14] where it was found that the average multiplicity from each jet production in $pp$ and $p\bar{p}$ collisions is usually larger than that in $e^+e^-$ annihilations. This contribution to particle production from initial and final state radiation is very important when one estimates the total $E_T$ production in ultrarelativistic heavy ion collisions where the number of minijets is enormous. We will discuss this in detail in a separate paper where we study jet production in heavy ion collisions.

The semi-inclusive pseudorapidity distributions $\rho_n(\eta) = (1/\sigma_\eta) d\sigma_n/d\eta$ for different multiplicity bins at $\sqrt{s}=200$ and 900 GeV are shown in Fig. 7. The agreement between our calculation (histograms) and the data [38] is satisfactory. As we will see later, large multiplicity events are dominated by minijet production. The corresponding central rapidity densities are higher and the distributions are narrower than the low multiplicity events, since most of the minijets are populated in the central rapidity region. Shown in Fig. 8 is the scaled central rapidity density $\rho_n(0)/\rho(0)$ as a function of the scaled multiplicity $n/\langle n \rangle$. We can see that there is an approximate scaling property in both the data and our model calculation, although the 10% energy variations in the model appear greater than in the data for large $n/\langle n \rangle \sim 3$.

## IV. TRANSVERSE-MOMENTUM DISTRIBUTIONS

As we have shown, jet production is negligible at low energies and only soft interactions with small $p_T$ transfer

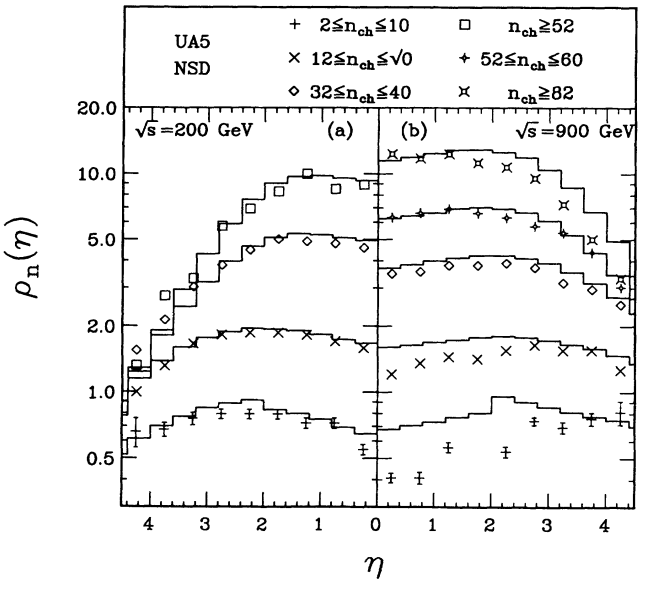


FIG. 7. HIJING results (histograms) and UA5 data [38] on the semi-inclusive pseudorapidity distributions for different multiplicity bins in NSD $p\bar{p}$ collisions at (a) $\sqrt{s}=200$ and (b) 900 GeV.

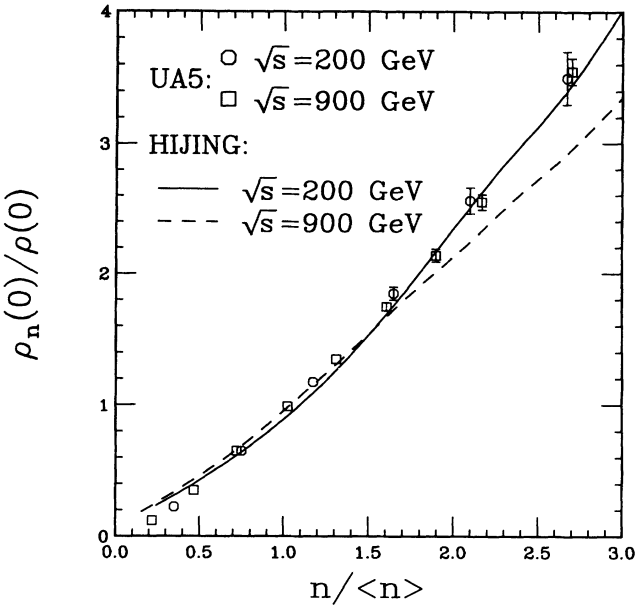


FIG. 8. Scaled central pseudorapidity density $\rho_n(0)/\rho(0)$ as a function of $n/\langle n \rangle$ in NSD $p\bar{p}$ collisions at $\sqrt{s}=200$ and 900 GeV. The lines are from HIJING calculation and the data are UA5 results [38].

are involved. In Fig. 9, we plot the $p_T$ spectra of produced particles in $pp$ collisions at $E_{\rm lab}=24$ and 200 GeV. We see that both our calculation (histograms) and the experimental data [35,43] show an exponential $p_T$ distribution characteristic of the fragmentation processes. In

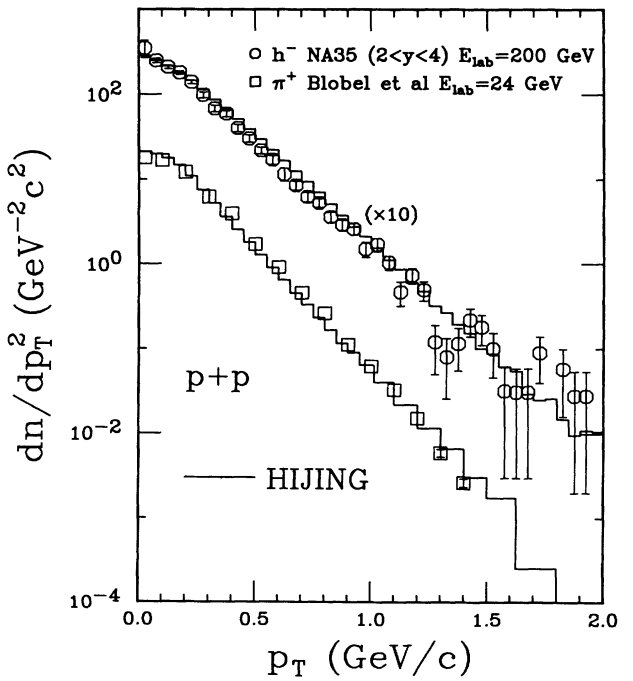


FIG. 9. $p_T$ distributions of $\pi^+$ in $pp$ collisions at $E_{\rm lab}=24$ GeV and negative particles at $E_{\rm lab}=200$ GeV. The histograms are HIJING results and the data are from Refs. [35,43].

HIJING we adopted a soft gluon radiation scheme as used in FRITIOF. However, we restrict the radiation to $p_T < p_0$. The resultant $p_T$ spectrum of produced particles still has an exponential form but the slope increases slightly with energy as can be seen from Fig. 9. In addition to the low-$p_T$ gluon radiation, HIJING also included an extra low $p_T < p_0$ transfer to the constituent quarks and diquarks at the string end points in soft interactions. We parametrize the probability for this transverse momentum kick by the form

$$f_{\text{kick}}(p_T) \propto \theta(p_0 - p_T)[(p_T^2 + c^2)(p_T^2 + p_0^2)]^{-1} , \quad (14)$$

where $c = 0.1$ GeV/$c$. This form was chosen to ensure that $f_{\text{kick}}(p_T)$ extrapolates smoothly to the regime of hard scattering while varying more slowly for $p_T \ll p_0$. With the default settings of Lund Monte Carlo program JETSET7.2, this extra small $p_T$ kick is necessary to fit the experimental data on $p_T$ distributions at low energies $E_{\text{lab}} \sim 20$ GeV. At these low energies, the effect of soft gluon radiation is very small. Without that small $p_T$ transfer, the transverse momentum from pair production in string fragmentation is not enough to account for the higher tail of the data at large $p_T$ [4]. For $E_{\text{lab}} \gtrsim 200$ GeV, Eq. (14) leads to much smaller effects.

At collider energies, jet production becomes more and more important. Since a large $p_T$ is always involved in jet production, the produced particles associated with jets must also carry large transverse momenta. Thus, the transverse momentum spectra of produced particles at large and intermediate $p_T$ should unequivocally manifest the presence of jet production. Shown in Fig. 10 are the invariant inclusive cross sections as a function of $p_T$ from HIJING calculation (histograms) as compared to the data [44–46] at collider energies from ISR up to Tevatron. Instead of being nearly an exponential function of $p_T$ at low energies as shown in Fig. 9, the $p_T$ distribution exhibits a clear power-law tail characteristic of PQCD. We have to keep in mind that soft physics is still dominant at low $p_T$. Only in addition to this background, PQCD jets develop a power-law tail at large $p_T$ and contribute to the low-$p_T$ particles as well. Here, the $p_T$ cutoff scale $p_0$ plays an important role in connecting our scheme for soft interactions with the hard or semihard PQCD processes. The successful reproduction of both the magnitude of the low-$p_T$ spectrum and the energy dependence of moderate high-$p_T$ tails is an important test for the overall consistency of our approach of combining the soft string phenomenology with hard QCD dynamics.

Another phenomenon associated with jet production in hadronic interactions is the correlation between average transverse momentum $\langle p_T \rangle$ and the total multiplicity [6,8,12]. As we shall show below, large multiplicity events are usually dominated by jet production. The average $p_T$ in these events is then larger than that of low multiplicity events. The competition between events with and without jets leads to the increase of $\langle p_T \rangle$ with charged multiplicity $n_{\text{ch}}$. We show in Fig. 11 the calculated correlation (histograms) between $\langle p_T \rangle$ and $n_{\text{ch}}$ as compared to the data [45] at $\sqrt{s} = 200$ and 900 GeV. HIJING reproduces the overall increase of $\langle p_T \rangle$ with $n_{\text{ch}}$

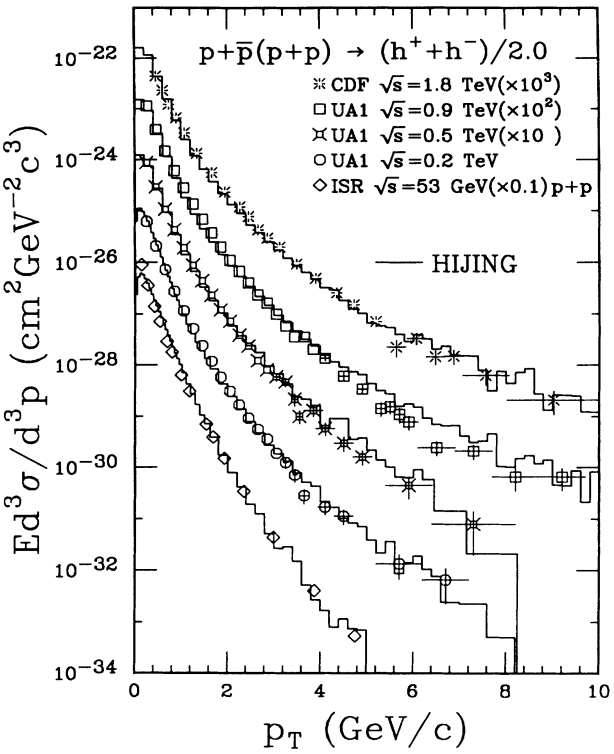


FIG. 10. Invariant inclusive cross sections of charged particles in $pp$ at $\sqrt{s} = 53$ GeV, $p\bar{p}$ collisions at $\sqrt{s} = 200$, 540, 900, and 1800 GeV. The histograms are HIJING results and the data are from Refs. [44–46]. Both the calculation and experimental data are obtained in the region of $|\eta| < 2.5$ for $\sqrt{s} = 200$, 540, and 900 GeV, and $|\eta| < 1.0$ for $\sqrt{s} = 5$ and 1800 GeV.

and $\sqrt{s}$. However, the precise shape is different from the data. This might be due to the particular string arrangement in HIJING, as the shape is quite sensitive to how the gluons are connected in the construction of string systems [18]. This may be one of the aspects of the model which may need further improvement in the future.

We also show in Fig. 12 the correlation between $\langle p_T \rangle$ and $n_{\text{ch}}$ for pions, kaons, and $\bar{p}$ (from bottom to top) respectively at $\sqrt{s} = 1800$ GeV. The solid histograms are direct HIJING calculations of $\langle p_T \rangle$. The dashed lines are obtained by the same procedure used in the experiment [47] in which the $p_T$ distributions are fitted with parametrizations [power law $a/(p_T + b)^n$ for pions and exponentials $c \exp(-\alpha p_T)$ for kaons and antiprotons] and the fitted parameters are used to calculate $\langle p_T \rangle$ in the range $0 < p_T < 1.5$ GeV/$c$. It is obvious that $\langle p_T \rangle$ for kaons and antiprotons are larger and the increases with $n_{\text{ch}}$ are faster than pions. This effect is mainly due to the finite mass of diquarks and strange quarks in the fragmentations of gluon jets which are dominant sources of minijet production at collider energies. The agreement of the calculated dependence of $\langle p_T \rangle$ vs $n_{\text{ch}}$ provides another strong piece of evidence supporting the role of multiple minijets. It shows that unconventional mechanisms such as in a hydrodynamic model [48], which attributes the different behavior of $\langle p_T \rangle$ vs $n_{\text{ch}}$ for different particles to the collective flow, are not needed to understand the

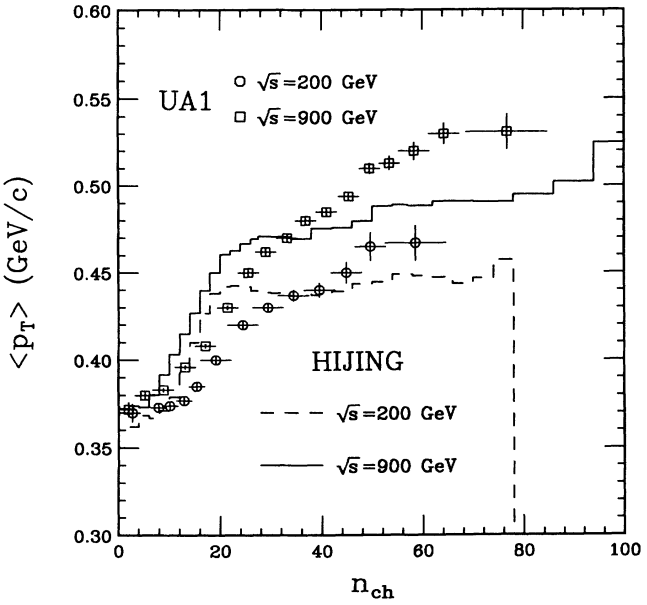


FIG. 11. UA1 data [45] and HIJING calculation (histograms) of the correlation between $\langle p_T \rangle$ (in $|\eta| < 2.5$) of charged particles and the total charged multiplicity.

present data. Rather, PQCD in the minijet regime seems to be adequate. The much better reproduction of the shape of the measured $p_T$ vs $n_{ch}$ in Fig. 12, where experimental biases are taken into account as compared to Fig. 11, suggests that the discrepancy in Fig. 11 may also be due to an inexact treatment of the experimental cuts in HIJING calculation for those data.

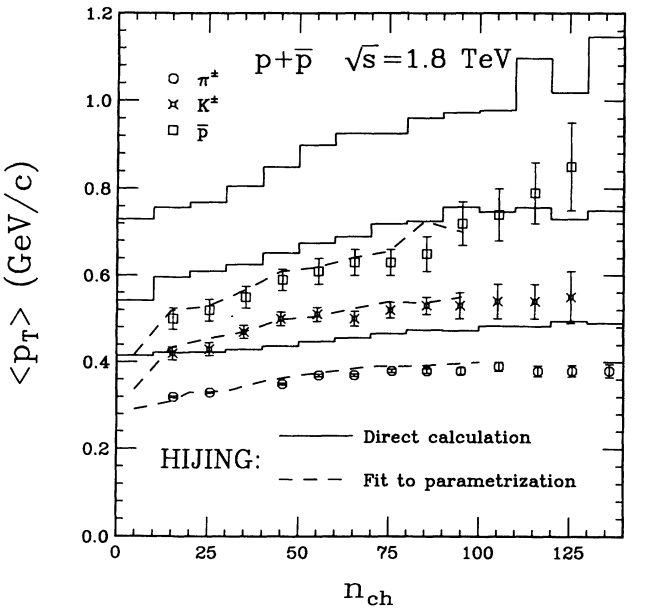


FIG. 12. $\langle p_T \rangle$ of pions, kaons, and antiprotons (from bottom to top) in $-0.36 < \eta < 1.0$ vs the charged multiplicity $n_{ch}$ in $|\eta| < 3.25$. The solid histograms are direct HIJING calculation and the dashed lines are obtained from parametrizations in the range $0 < p_T < 1.5$ which are fitted to the calculation via the experimental procedures used to obtain the data points [47].

## V. MULTIPLICITY DISTRIBUTIONS

So far we have been discussing the inclusive distributions of produced particles. We have demonstrated the important role of multiple minijet production in these distributions. We have also seen the correlations between the inclusive distributions and the total charged multiplicity of the events. The study of multiplicity distributions is therefore illustrative to understand the underlying event structure in terms of jet production.

In Figs. 13 and 14, we show the total charged multiplicity distributions from HIJING and the corresponding data [49–51] at $\sqrt{s} = 53$, 200, 546, and 900 GeV. There is a systematic widening of the distributions with colliding energies. Also shown in the figures are the contributions to the multiplicity distribution from events with no jet production (dot-dashed histograms), one jet production (dashed histograms), and two or more jet production (dotted histograms). We note that at $\sqrt{s} = 53$ GeV, jet production is barely visible. However at higher energies, events with one or more than one jet production are becoming increasingly important and are finally dominant among those events with large multiplicity. All the low multiplicity events are dominated by those of no jet

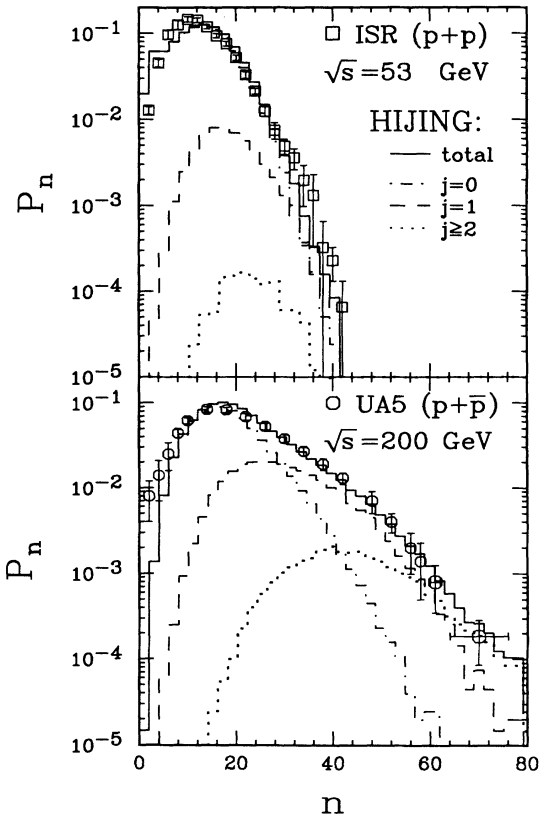


FIG. 13. Charged multiplicity distributions in NSD $pp$ at $\sqrt{s} = 53$ GeV and $p\bar{p}$ collisions at $\sqrt{s} = 200$ GeV. The data are from Refs. [49,50]. The solid histograms are from HIJING calculation with contributions from events with $j = 0$ (dot-dashed histograms), $j = 1$ (dashed histograms), and $j \geq 2$ (dotted histograms) number of jet production.

production. Therefore, we can see that it is the increasing number of jet production that causes the multiplicity distributions to become wider and then the violation of KNO scaling [14]. As we have shown earlier, the population of jet production in different multiplicity events is also responsible for the decrease of the rapidity distribution width (see Fig. 7) and the increase of $\langle p_T \rangle$ (see Figs. 11 and 12) with $n_{\rm ch}$.

The multiplicity distributions for charged particles in different pseudorapidity intervals are shown in Fig. 15. The agreement between the HIJING calculation and the data [50] is again very good. One should remember that the seemingly narrower distribution for the smaller $\eta$ interval is an artifact of small average multiplicity. If shown in a KNO plot, the fluctuation in $n/\langle n \rangle$ increases with narrower rapidity bins.

## VI. KAON AND BARYON PRODUCTION

While HIJING uses PYTHIA subroutines to generate the kinetic variables of scattered partons in each hard scattering, some simplifications have been made in order to generalize jet production to the cases of $pA$ and $AA$ collisions. One assumption we made is about the color flow in hard processes. Even though a consistent scheme can be derived [52] to a certain approximation in events with one hard scattering, the color arrangement in multiple jet production events can be very complex. However, it was found that the final inclusive distributions are fortunately not sensitive to the actual parton ordering [18]. In HIJING, we simply assign one of the two scattered partons and the associated ones from radiation to a given participant nucleon. After all hard scatterings are performed, the produced partons are connected to the valence quark and diquark of their assigned nucleon to form a color singlet string system which is then fragmented into hadrons. For rare processes which produce a $q\bar{q}$ pair in the final state, the quark and antiquark will form a single string system. To be consistent with our treatment of soft excitations and to conserve flavor, we also assumed that each nucleon can only have one hard scattering which involves quarks or antiquarks (except $q\bar{q}$ scatterings). After this scattering, the subsequent ones are restricted to gluon-gluon scatterings. The flavor of the final scattered quarks or antiquarks are replaced by one of the valence quarks to fix the color flow. This prescription leads to a small error for flavor correlation but retains the correct rate and kinematics of those PQCD processes.

To check the flavor composition of produced particles in HIJING given the above simplifications, we show in Fig. 16 the calculated pseudorapidity distributions for kaons (lines) at two collider energies, $\sqrt{s}=200$ and 900 GeV. The data are from UA5 experiments [53]. The agreement between our calculation and the data in the central rapidity region is satisfactory. The discrepancy at large

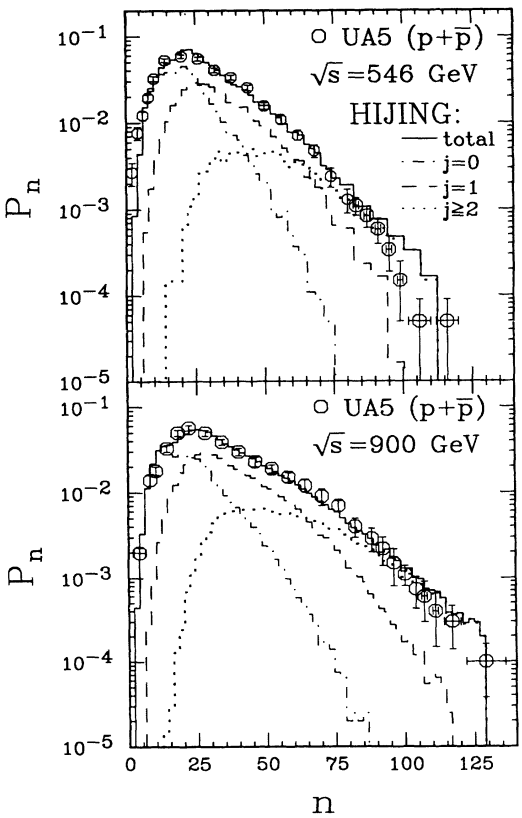


FIG. 14. Same as Fig. 13, but for NSD $p\bar{p}$ collisions at $\sqrt{s}=546$ and 900 GeV. The data are from Refs. [50,51].

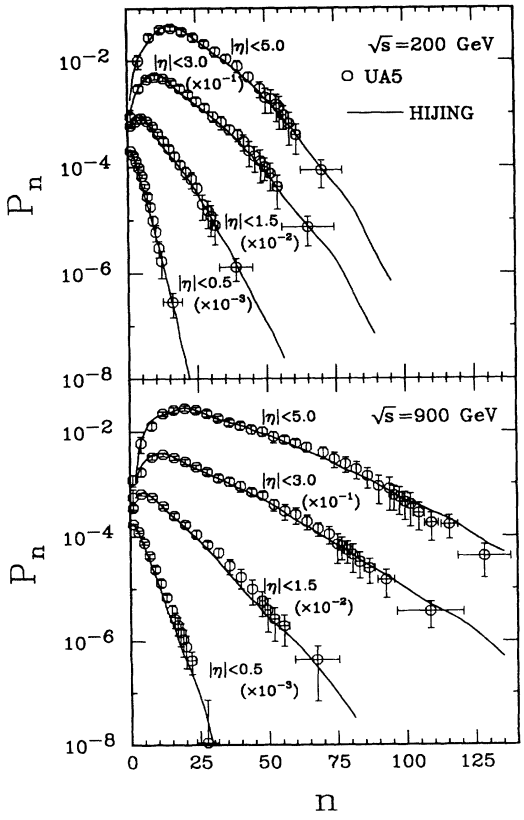


FIG. 15. Multiplicity distributions for charged particles in different rapidity intervals in NSD $p\bar{p}$ collisions at $\sqrt{s}=200$ and 900 GeV. The data are from Ref. [50] and the lines are from HIJING calculation.

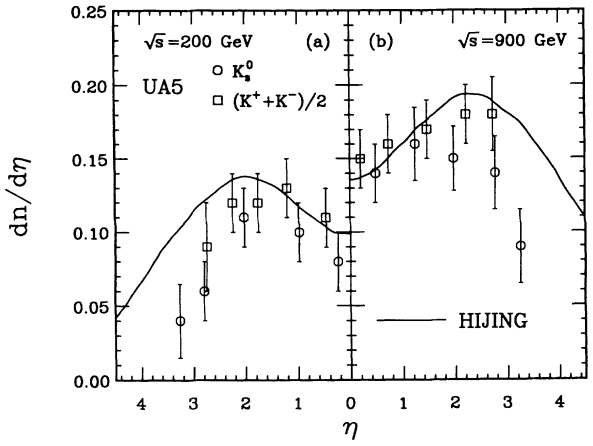


FIG. 16. HIJING calculation (lines) of pseudorapidity distributions of kaons in $p\bar{p}$ collisions at (a) $\sqrt{s}=200$ and (b) 900 GeV as compared to UA5 data [53].

values of $|\eta|$ might be due to the experimental acceptance or the diquark fragmentation scheme we use. Figure 17 shows the $p_T$ spectra of pions, kaons, and antiprotons in the central region of $p\bar{p}$ collisions at $\sqrt{s}=1800$ GeV. For kaons and antiprotons, the distributions are flatter at large $p_T$ than pions and tend to saturate faster at small $p_T$. This leads to a larger $\langle p_T \rangle$ for kaons and antiprotons as shown in Fig. 12 as well as an increase of the $K/\pi$ or $\bar{p}/\pi$ ratio with $p_T$. Note that simple parametrizations of the high-$p_T$ data extrapolated down to small $p_T$ lead to the large systematic effects as seen in Fig. 12 between the direct calculation and experimental points.

The $K/\pi$ ratio in the central rapidity region as a function of $p_T$ is shown in Fig. 18 with UA5 data [54] at $\sqrt{s}=540$ GeV. We see that the model reproduces the data well. We have checked that the $K/\pi$ ratio at moderate $p_T$ is not sensitive to the colliding energy. The invariant cross section of baryons to that of pions in the central rapidity region is shown in Fig. 19. The data are from UA2 experiments [55]. There is no experimental data available on leading valence baryon distributions at

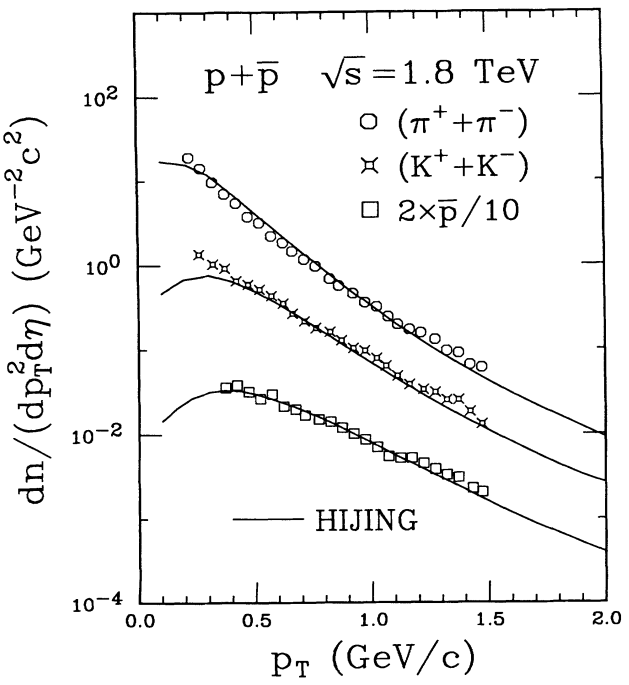


FIG. 17. $p_T$ spectra of pions, kaons, and antiprotons ($-0.36<\eta<1.0$) in $p\bar{p}$ collisions at $\sqrt{s}=1.8$ TeV as calculated by HIJING model (solid lines). The data are from Ref. [47].

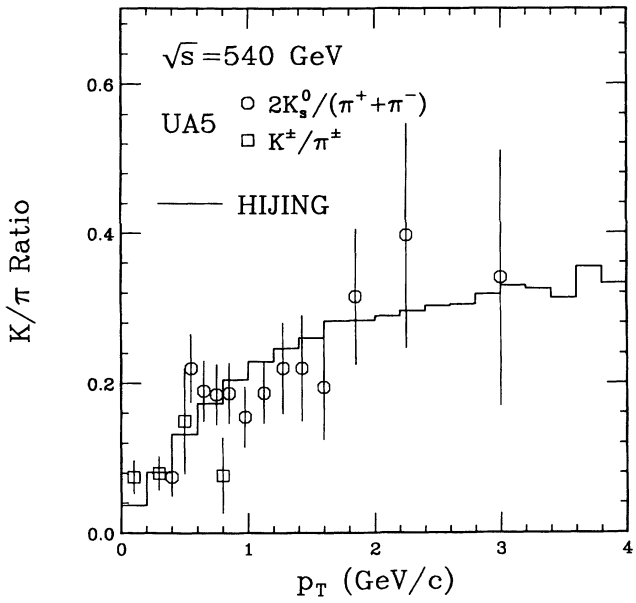


FIG. 18. Ratio of invariant cross sections of kaons to that of pions as a function of $p_T$ in the central region $|\eta|<2.5$ of $p\bar{p}$ collisions at $\sqrt{s}=540$ GeV. The data are from Ref. [54] and histogram is HIJING calculation.

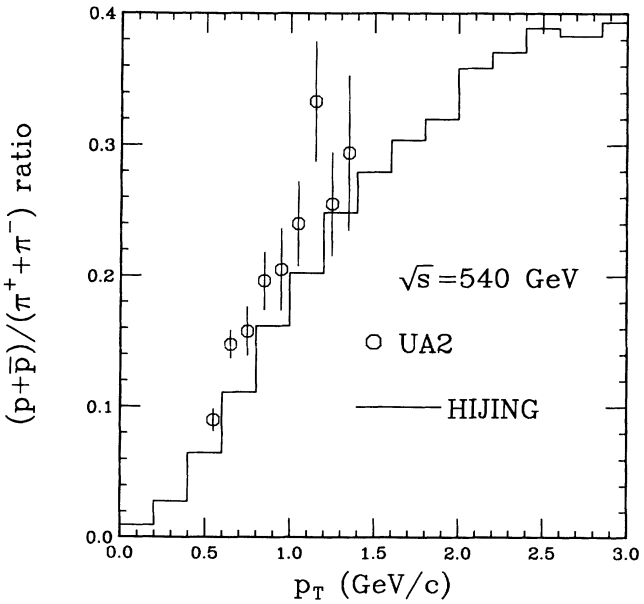


FIG. 19. Ratio of invariant cross sections of protons and antiprotons to that of pions as a function of $p_T$ in the central region $|\eta|<2.5$ of $p\bar{p}$ collisions at $\sqrt{s}=540$ GeV. The data are from Ref. [55] and histogram is HIJING calculation.

collider energies. As we have checked at low energies in Ref. [4], HIJING does not reproduce well the leading baryon rapidity distributions. This could stem from the diquark fragmentation scheme in JETSET7.2. A better agreement with the leading baryon distribution data can be achieved by introducing another fragmentation function and an additional diffractive mechanism involving sea quark-antiquark strings as in the DPM [15]. In the present version of HIJING, these mechanisms are not implemented.

## VII. TWO-PARTICLE CORRELATIONS

In the above sections we have studied single inclusive particle distributions. However, investigations of correlations among final state particles are also important in order to reveal further properties of the underlying production mechanism. Especially in the wake of increasing interest in the intermittent fluctuation of multiparticle production [56], multiple particle correlations have been proven [57] to play important roles in understanding the observed intermittency in high energy hadronic interactions. It has been shown [58] that particles from jet fragmentation in hadronic interactions have intermittent behaviors in small rapidity bins. A detailed study of this aspect is beyond the scope of this paper. Instead, we concentrate in this section on two-particle correlations in different rapidity bins and how they are influenced by jet production.

The most common models to explain the observed two-particle correlation are clusters models [59], in which the final state particles are created by the isotropic decay of clusters. From a general point of view, the fragmentation of jets can also be regarded as the decay of clusters with a constant rapidity width of about one as determined by the experimental study of jet profiles [42]. It is not hard to imagine that jet production in hadronic interactions should bring enhancement to short range correlations of two-particle production, since particles from jet fragmentation tend to cluster together in phase space. Furthermore, jet production must also introduce long range correlations as each hard scattering produces a forward and backward pair of scattered partons.

The two-particle correlation function is defined as

$$C(\eta_1,\eta_2)=\rho(\eta_1,\eta_2)-\rho(\eta_1)\rho(\eta_2)\ , \tag{15}$$

where $\rho(\eta_1,\eta_2)$ is the two-particle density which is proportional to the probability of joint particle production at $\eta_1$ and $\eta_2$. Similarly one can define the semi-inclusive two-particle correlation function $C_n(\eta_1,\eta_2)$ for events with fixed multiplicity $n$. An intrinsic correlation function can be expressed in terms of $C_n(\eta_1,\eta_2)$ as

$$C_S(\eta_1\cdot\eta_2)=\sum_n \frac{\sigma_n}{\sigma} C_n(\eta_1,\eta_2)\ . \tag{16}$$

This correlation function is usually referred to as "short-range" contribution to $C(\eta_1\eta_2)$ as we will see below that it is sharply peaked at $\eta_1=\eta_2$.

We plot our calculated $C(\eta_1,\eta_2)$ and $C_S(\eta_1,\eta_2)$ (solid lines) in Fig. 20 together with the UA5 data [60] at

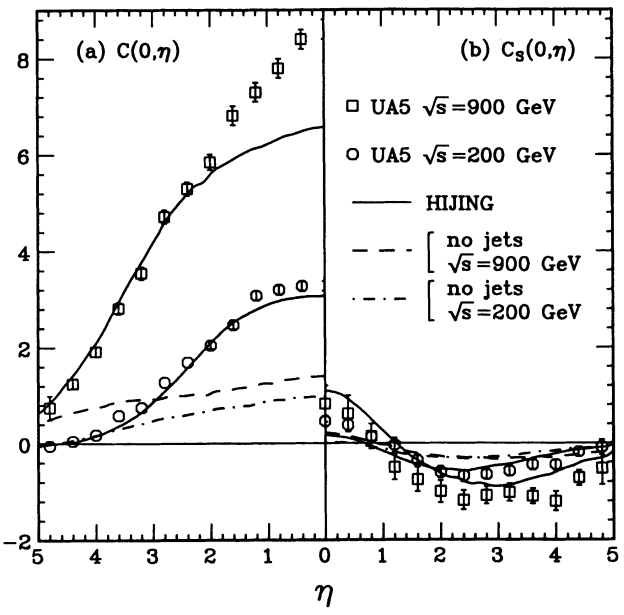


FIG. 20. Two-particle correlation function (a) $C(\eta_1,\eta)$ and (b) its "short-range" component $C_S(\eta_1,\eta)$ at fixed $\eta_1=0$ vs $\eta$ in $p\bar{p}$ collisions at $\sqrt{s}=200$ and 900 GeV. Solid lines are from HIJING calculation and the data are from Ref. [60]. The dot-dashed and dashed lines are HIJING results without jet production at $\sqrt{s}=200$ and 900 GeV, respectively.

$\sqrt{s}=200$ and 900 GeV. Also plotted as dashed and dot-dashed lines are the correlation functions for events without jet production. We can see that the two-particle correlation function $C(\eta_1,\eta_2)$ in Fig. 20(a) is dominated by the contributions from jet production. It increases with energy faster than the single-particle density $\rho(\eta)$. By definition, the "short-range" component $C_S(\eta_1,\eta_2)$ of the correlation function filters out the mixing of events with different multiplicities which can cause strong correlations. It thus has smaller values and is less energy dependent, as shown in Fig. 20(b). The 30% underprediction of HIJING at $\eta=0$ at $\sqrt{s}=900$ GeV is not understood at present.

The long range or forward-backward correlation can be studied by looking at particle production in two rapidity bins with equal size but separated by a rapidity gap $\Delta\eta$. Let us define the number of charged particles with rapidities between $\Delta\eta/2$ and $\Delta\eta/2+1$ as $n_F$ and those between $-\Delta\eta/2$ and $-(\Delta\eta/2+1)$ as $n_B$. For a symmetrical system, i.e., $\langle n_B\rangle=\langle n_F\rangle$ and $\langle n_B^2\rangle=\langle n_F^2\rangle$, the forward-backward correlation strength is defined as

$$b=\frac{\langle n_F n_B\rangle-\langle n_F\rangle^2}{\langle n_F^2\rangle-\langle n_F\rangle^2}\ . \tag{17}$$

As shown in Fig. 21, HIJING (solid histogram) reproduces the variation of $b$ with $\Delta\eta$ and its energy dependence. However, without jet production, the forward-backward correlation is too weak as compared to the experimental data [60].

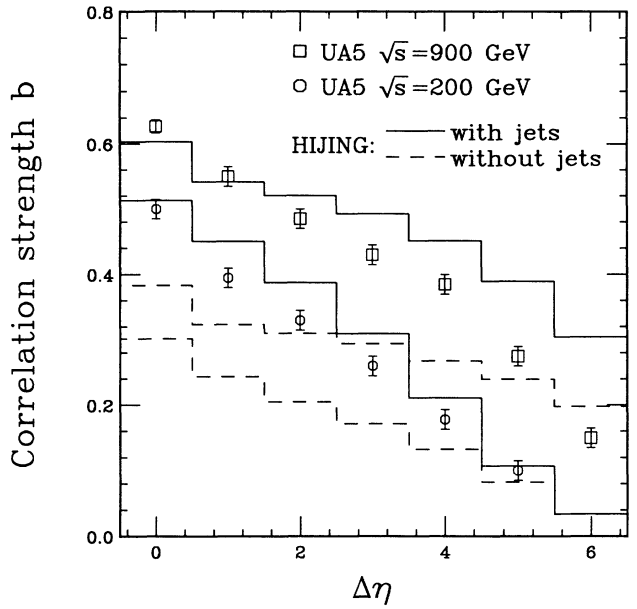


FIG. 21. Forward-backward correlation strength $b$ vs the rapidity gap $\Delta\eta$ as calculated by HIJING with (solid histograms) and without (dashed histograms) jet production. The data are from Ref. [60].

## VIII. CONCLUSIONS AND REMARKS

In this paper, we have made a systematic study of particle production in $pp$ and $p\bar{p}$ collisions in the energy range of $\sqrt{s}=5-2000$ GeV, using the HIJING Monte Carlo model [4] developed for high energy $pp$, $pA$, and $AA$ collisions. We have achieved satisfactory agreement with experimental data not only on single inclusive distributions, e.g., rapidity and transverse momentum distributions, but also on the global features of events (multiplicity fluctuation and the energy dependence of central rapidity density) and two-particle correlations. We have demonstrated that multiple jet production is increasingly important in every aspect of particle production at collider energies. Our results indicate that multiple minijets provide a consistent explanation of the increase of the central rapidity density, the development of power-law tail of the transverse-momentum spectra, the widening of multiplicity distributions, and the enhancement of both short and long range two-particle correlations with increasing energies. Initial and final state radiation associated with jet production is also found to have significant effects in particle production.

As in many other models [18,19] that have attempted to merge low- and high-$p_T$ dynamics, we have introduced a $p_T$ cutoff scale $p_0$, which we regard as a model dependent phenomenological parameter separating the PQCD dynamics at high $p_T$ from the nonperturbative low-$p_T$ regime. The value $p_0=2$ GeV/$c$ was chosen by fitting the high energy $pp$ and $p\bar{p}$ cross sections assuming an asymptotic constant cross section for soft processes [14]. This also leads to the correct energy dependence of $dn/d\eta$ ($\eta=0$) with a constant contribution from soft processes. This assumption about the energy independence of soft processes at high energies allows us to model the nonperturbative processes with $p_T<p_0$ with a simple string phenomenology. Otherwise a more complex soft phenomenology with more parameters and assumptions would have to be introduced. It is fortunate and important for the overall consistency of the model that $p_0=2$ GeV/$c$ is also sufficiently large for the application of PQCD at $p_T\geq p_0$ [5–14].

While many aspects of multiparticle dynamics used in HIJING have been discussed separately in previous works [15,16,18], our goal with HIJING was to combine them together in a consistent framework with a minimum number of parameters. We have shown that HIJING provides a comprehensive explanation of a broad spectrum of data on $pp$ and $p\bar{p}$ reactions in a wide energy range. In addition, our study of particle production in this paper is vital for our extrapolation to $pA$ and $AA$ collisions [20] since we have shown that the existing $A=1$ data at collider energies is well reproduced.

## ACKNOWLEDGMENTS

We would like to thank B. Andersson, F. Paige, J. Harris, P. Jacobs, M. A. Bloomer, and A. Poskanzer for helpful comments. We also thank T. Sjöstrand for making available the Monte Carlo program PHYTIA. This work was supported by the Director, Office of Energy Research, Division of Nuclear Physics of the Office of High Energy and Nuclear Physics of the U.S. Department of Energy under Contract No. DE-AC03-76SF00098.

[1] K. Kajantie, P. V. Landshoff, and J. Lindfors, Phys. Rev. Lett. **59**, 2517 (1987); K. J. Eskola, K. Kajantie, and J. Lindfors, Nucl. Phys. **B323**, 37 (1989); G. Calucci and D. Treleani, Phys. Rev. D **41**, 3367 (1990).

[2] E. V. Shurak, Phys. Rep. **61**, 71 (1980); L. McLerran, Rev. Mod. Phys. **58**, 1021 (1986); see also articles in *Quark Matter 90,* Proceedings of the Conference, edited by J. P. Blaizot *et al.* [Nucl. Phys. **A525**, 1c (1991)].

[3] M. Gyulassy and M. Plümer, Phys. Lett. B **243**, 432 (1990).

[4] X. N. Wang and M. Gyulassy, Phys. Rev. D **44**, 3501 (1991).

[5] A. Capella and J. Tran Thanh Van, Z. Phys. C **23**, 165 (1984).

[6] T. K. Gaisser and F. Halzen, Phys. Rev. Lett. **54**, 1754 (1985).

[7] P. l'Heureux *et al.,* Phys. Rev. D **32**, 1681 (1985).

[8] G. Pancheri and Y. N. Srivastava, Phys. Lett. B **182**, 199 (1986).

[9] L. Durand and H. Pi, Phys. Rev. Lett. **58**, 303 (1987); Phys. Rev. D **38**, 78 (1988).

[10] J. Dias de Deus and J. Kwiecinski, Phys. Lett. B **196**, 537 (1987).

[11] R. C. Hwa, Phys. Rev. D **37**, 1830 (1988).

[12] X. N. Wang and R. C. Hwa, Phys. Rev. D **39**, 187 (1989).

[13] T. K. Gaisser, F. Halzen, and A. D. Martin, Phys. Lett.

**166B**, 219 (1986).
[14] X. N. Wang, Phys. Rev. D **43**, 104 (1991).
[15] A. Capella, U. Sukhatme, and J. Tran Thanh Van, Z. Phys. C **3**, 329 (1980); J. Ranft, Phys. Rev. D **37**, 1842 (1988); Phys. Lett. B **188**, 379 (1987).
[16] B. Andersson, G. Gustafson, and B. Nilsson-Almqvist, Nucl. Phys. **B281**, 289 (1987); B. Nilsson-Almqvist and E. Stenlund, Comput. Phys. Commun. **43**, 387 (1987).
[17] F. E. Paige and S. D. Protopopescu, in *Physics of the Superconducting Super Collider, Snowmass, 1986,* Proceedings of the Summer Study, Snowmass, Colorado, edited by R. Donaldson and J. Marx (Division of Particles and Fields of the APS, New York, 1987), p. 320.
[18] T. Sjöstrand and M. van Zijl, Phys. Rev. D **36**, 2019 (1987); T. Sjöstrand, Comput. Phys. Commun. **39**, 347 (1986); T. Sjöstrand and M. Bengtsson, *ibid.* **43**, 367 (1987).
[19] T. K. Gaisser and T. Stanev, Phys. Lett. B **219**, 375 (1989).
[20] X. N. Wang, LBL Report LBL-29390 (1991); M. Gyulassy, M. Plümer, M. Thoma, and X. N. Wang, in Proceedings of the Fourth Conference on the Intersections between Particle and Nuclear Physics, Tucson, Arizona, 1991 (to be published).
[21] M. Gyulassy, in *Proceedings of Eighth Balaton Conference on Nuclear Physics,* edited by Z. Fodor (KFKI, Budapest, 1987); CERN Report CERN-TH-4794/87, 1987 (unpublished).
[22] J. Dias de Deus, Nucl. Phys. **B59**, 231 (1973); **B252**, 369 (1985).
[23] E. Eichten, I. Hinchliffe, K. Lane, and C. Quigg, Rev. Mod. Phys. **56**, 579 (1984).
[24] D. W. Duke and J. F. Owens, Phys. Rev. D **30**, 50 (1984).
[25] P. N. Harriman, A. D. Martin, W. J. Stirling, and R. G. Roberts, Phys. Rev. D **42**, 798 (1990).
[26] P. V. Landshoff and J. C. Polkinghorne, Phys. Rev. D **18**, 3344 (1978); C. Goebel, D. M. Scott, and F. Halzen, *ibid.* **22**, 2789 (1980); B. Humpert, Phys. Lett. **131B**, 461 (1983); N. Paver and D. Treleani, *ibid.* **146B**, 252 (1984).
[27] U. Amaldi and K. R. Schubert, Nucl. Phys. **B166**, 301 (1980).
[28] UA4 Collaboration, M. Bozzo *et al.,* Phys. Lett. **147B**, 392 (1984).
[29] UA5 Collaboration, G. J. Alner *et al.,* Z. Phys. C **32**, 153 (1986).
[30] Fermilab E710 Collaboration, N. Amos *et al.,* Phys. Rev. Lett. **63**, 2784 (1989).
[31] R. M. Baltrusaitis *et al.,* Phys. Rev. Lett. **52**, 1380 (1984).
[32] T. Hara *et al.,* Phys. Rev. Lett. **50**, 2058 (1983). The *pp* cross sections converted from *p*-air data are taken from L. Durand and H. Pi, Phys. Rev. Lett. **58**, 303 (1987).
[33] J. K. Gunion and G. Bertsch, Phys. Rev. D **25**, 746 (1982).
[34] B. Andersson, G. Gustafson, G. Ingelman, and T. Sjöstrand, Phys. Rep. **97**, 31 (1983); T. Sjöstrand, Comput. Phys. Commun. **27**, 243 (1982).
[35] Bonn-Hamburg-München, Collaboration, V. Blobel *et al.,* Nucl. Phys. **B69**, 454 (1974).
[36] C. De Marzo *et al.,* Phys. Rev. D **26**, 1019 (1982).
[37] K. Goulianos, Phys. Rep. **101**, 169 (1983).
[38] UA5 Collaboration, G. J. Alner *et al.,* Z. Phys. C **33**, 1 (1986).
[39] F. Abe *et al.,* Phys. Rev. D **41**, 2330 (1990).
[40] W. Thomé *et al.,* Nucl. Phys. **B129**, 365 (1977).
[41] J. Whitemore *et al.,* Phys. Rep. **10C**, 273 (1974); W. M. Morse *et al.,* Phys. Rev. D **15**, 66 (1977); C. P. Ward *et al.,* Nucl. Phys. **B153**, 299 (1979).
[42] UA1 Collaboration, C. Albajar *et al.,* Nucl. Phys. **B309**, 405 (1988).
[43] NA35 Collaboration, H. Ströbele *et al.,* Z. Phys. C **38**, 89 (1988).
[44] British-Scandinavian Collaboration, B. Alper *et al.,* Nucl. Phys. **B87**, 19 (1975).
[45] UA1 Collaboration, C. Albajar *et al.,* Nucl. Phys. **B335**, 261 (1990).
[46] F. Abe *et al.,* Phys. Rev. Lett. **61**, 1819 (1988).
[47] T. Alexopoulos *et al.,* Phys. Rev. Lett. **64**, 991 (1990).
[48] Péter Lévai and Berndt Müller, Phys. Rev. Lett. **67**, 1519 (1991).
[49] ABCDHW Collaboration, A. Breakstone *et al.,* Phys. Rev. D **30**, 528 (1984).
[50] UA5 Collaboration, R. E. Ansorge *et al.,* Z. Phys. C **43**, 357 (1989).
[51] UA5 Collaboration, G. J. Alner *et al.,* Phys. Rep. **154**, 247 (1987).
[52] G. Gustafson, Z. Phys. C **15**, 155 (1982).
[53] UA5 Collaboration, R. E. Ansorge *et al.,* Z. Phys. C **41**, 179 (1988).
[54] UA5 Collaboration, G. J. Alner *et al.,* Nucl. Phys. **B258**, 505 (1985).
[55] UA2 Collaboration, M. Banner *et al.,* Phys. Lett. **122B**, 322 (1983).
[56] A. Białas and R. Peschanski, Nucl. Phys. **B273**, 703 (1986).
[57] P. Carruthers and I. Sarcevic, Phys. Rev. Lett. **63**, 1562 (1989).
[58] X. N. Wang, Phys. Lett. B **248**, 447 (1990).
[59] E. L. Berger, Nucl. Phys. **B85**, 61 (1975); J. Benecke and J. Kühn, *ibid.* **B140**, 179 (1978).
[60] UA5 Collaboration, R. E. Ansorge *et al.,* Z. Phys. C **37**, 191 (1988).